Influence of granular temperature and grain rotation on the wall friction coefficient in confined shear granular flows

Cheng-Chuan Lin[1,*], *Riccardo* Artoni[2,**], *Fu-Ling* Yang[1,3,***], and *Patrick* Richard[2,****]

[1]Department of Mechanical Engineering, National Taiwan University, Taipei, Taiwan
[2]MAST-GPEM, Univ Gustave Eiffel, IFSTTAR, 44344, Bouguenais, France
[3]Center for Advanced Study in Theoretical Sciences (CASTS), National Taiwan University, Taipei, Taiwan

Abstract. A depth-weakening wall friction coefficient, μ_w, has been reported from three-dimensional numerical simulations of steady and transient dense granular flows. To understand the degradation mechanisms, a scaling law for μ_w/f and χ has been proposed where f is the intrinsic particle-wall friction and χ is the ratio of slip velocity to square root of granular temperature (Artoni & Richard, *Phys. Rev. Lett.*, vol. 115 (15), 2015, 158001). Independently, a friction degradation model has been derived which describes a monotonically diminishing friction depends on a ratio of grain angular and slip velocities, Ω (Yang & Huang, *Granular Matter*, vol. 18 (4), 2016, 77). In search of experimental evidence for how these two parameters degrade the μ_w, an annular shear cell experiment was performed to estimate the bulk granular temperature, angular and slip velocities at sidewall through image-processing. Meanwhile, μ_w was measured by a force sensor to confirm the weakening towards the creep zone. The measured $\mu_w/f-\chi$ and $\mu_w/f-\Omega$ were both well-fitted to the corresponding models showing that both granular temperature and angular velocity are significant mechanisms to degrade the μ_w which broadens the research perspective on modeling the boundary condition of dense granular flows.

1 Introduction

Extensive research effort has been made on developing feasible constitutive models for dense granular flows, the boundary condition plays an equally important role for the comprehension of many geophysical phenomena and industrial applications but has been less investigated. Two types of basal boundary conditions are often assumed in the literature: the no-slip [1–5] and slip [6–10] velocity conditions. For the lateral boundary, however, the solid nature of grains suggests the Coulomb-type stress of $\tau_w = \mu_w p$ with a constant *effective wall friction coefficient* μ_w and an assumed hydrostatic pressure p [11–14].

In fact, non-constant and flow-dependent effective wall friction coefficient has been reported from recent three-dimensional discrete element simulations [15–19]. The weakening of μ_w towards the creep zone is a robust feature as long as the particle-wall friction coefficient, f, in the simulation contact model is sufficiently large.

Researchers have proposed different explanations for this phenomenon. For example, Richard et al. [15] discussed the force cancellation mechanism when individual grains exhibit velocity fluctuations in random directions instead of conforming uniformly to the bulk streamwise velocity $u_\parallel$. A diminishing μ_w thus is attributed to a promoted degree of random fluctuations which is characterized by a dimensionless variable $\chi = u_\parallel/\sqrt{T_\parallel}$ in terms of the ratio of $u_\parallel$ to the streamwise granular temperature. Later on, Artoni and Richard [17] extracted simulation data from a steady confined shear flow to fit

$$\frac{\mu_w}{f} = \frac{\chi^B}{A+\chi^B} \tag{1}$$

with two fitting constants A and B.

Independently, Yang and Huang [18] attribute the degradation of μ_w to grain rotation based on the observation in granular avalanche experiments with lateral confinement. When a grain moves relative to the container wall at a translation velocity vector $\boldsymbol{u}_{pi}$, its rotation at $\boldsymbol{\omega}_{pi}$ diverts the sliding friction force against $\boldsymbol{u}_{pi}+\boldsymbol{R}\times\boldsymbol{\omega}_{pi}$ at the contact point. As a grain rotates under unbalanced torque from interactions with the neighbor grains, the resultant $\boldsymbol{\omega}_{pi}$ direction shall be random so does the diversion of friction. The individual friction force vectors hence can cancel out to give a lower bulk value against the bulk velocity $u_\parallel$. The degree of diversion and hence the friction degradation is characterized by a dimensionless rotation index, $\Omega = |\boldsymbol{\omega}|D/2u_\parallel$ with a mean angular speed $|\boldsymbol{\omega}| = \langle|\boldsymbol{\omega}_{pi}|\rangle$. The authors derived a formula for how μ_w is degraded based on the dynamics of a single grain as

$$\frac{\mu_w}{f} = \frac{1+a\Omega}{\sqrt{(1+a\Omega)^2+(b\Omega)^2}}. \tag{2}$$

Here, the coefficients $a = \omega_\perp/|\boldsymbol{\omega}|$ and $b = \omega_\parallel/|\boldsymbol{\omega}|$ ($-1 \le a$, $b \le 1$) represents the bulk angular velocity component in the direction perpendicular and parallel to bulk motion $u_\parallel$,

*e-mail: f00522316@ntu.edu.tw
**e-mail: riccardo.artoni@univ-eiffel.fr
***e-mail: fulingyang@ntu.edu.tw
****e-mail: patrick.richard@univ-eiffel.fr
A video is available at https://doi.org/10.48448/gt5c-my19

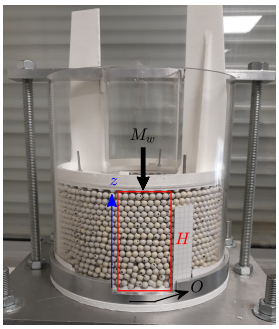

Figure 1. Experiment setup for annular shear cell containing marked spheres. Various loadings M_w are imposed on top wall while the bottom plate rotating at different rates O.

respectively, and hence have their physics origin. Despite the difference in model formulation, both Eq. (1) and Eq. (2) describe a monotonically decaying μ_w/f with the associated parameters χ and Ω and this work aims to provide the first experimental evidence for both models. In Sec. 2, we describe the experiment setup, the image processing methods for grain dynamics. The force measurement results and the resulting μ_w, the post analysis for bulk variables and the associated χ and Ω will be presented in Sec. 3. Finally, we conclude this study in Sec. 4.

2 Experiment setup and image processing methods

2.1 Facility and flow conditions

The current experiment setup was prepared according to [20]. A total amount of 2.1 kg of nearly identical Polyoxymethylene (POM) spheres with diameter $D = 5.9 \pm 0.1$ mm were filled into the annular shear cell to a height $H = 15D$ as shown in Fig. 1. Each sphere has a nearly circular mark of diameter 1 mm on the surface. The bottom bumpy wall can be driven by a stepper motor rotating at three different rates, $O = 5.9, 23.4$ and 117.2 r.p.m while the top bumpy wall was loaded with various weights, $M_w = 0.22$, 1.1 and 5.4 kg. A lateral high speed camera (Phantom Miro 320S) was used to record the flow process from the cell boundary (red box in Fig. 1) at different frame rates from 24 to 3400 FPS. Two homogeneous light-emitting diode (LED) panels (FOTGA LED430) were placed by the sides of the camera to provide sufficient illumination. In addition, a LED lamp (EFFILux EFFISharp) was used to generate a reflective bright spot on the sphere surface to permit particle tracking. All the examined flow conditions with different top weights M_w and rotating rates O are listed in Table. 1.

2.2 Image processing for grain dynamics

In order to study the grain translation and rotation dynamics during a flow process, the sphere center and its corresponding marker positions are required. Firstly, nearly circular bright spots from LED panel reflection were generated on roughly the same location on the sphere surface in the raw gray-scale images. A Circular Hough transformation [21] was then applied to identify each bright spots after employing a low-pass Gaussian filter and a Laplacian of Gaussian (LOG) filter. The deviation vector from the located spot position to the sphere actual center was evaluated by manually fitting a circle to the sphere circumference. The mean deviation distance scaled by the sphere diameter was found, $\Delta r/D = 0.09 \pm 6.1 \times 10^{-3}$, with a deviation from the horizontal line, $\theta = 1.15 \pm 0.09$ (rad). Averaging over all spheres in one image, the coefficient of variation falls below 8% and hence may be treated as uniform across the image. Hence, we moved the spot centers according to these offset values to locate the true sphere center (C_{Mx}, C_{My}) throughout the whole images as the illumination and camera setup remained unchanged.

Once the sphere center was located, a searching circle of radius $D/2$ was extended from sphere center to find the corresponding marker pixels in the image coordinate (x, y). In each searching circle, the pixels of position (x_{pi}, y_{pi}) whose gray-scale index falls below a specified critical value were identified as the marker pixels and the marker position was hence represented by the average pixel position of a total amount of N marker pixels as $(x_m, y_m) = (\sum_i x_{pi}/N, \sum_i y_{pi}/N)$.

The sphere and marker locations in consecutive images are then traced by the nearest neighbor method [21]. The five consecutive marker positions $S_{k=1-5}(x_{mk}, y_{mk})$ within one sphere were moved to the sphere-fitted coordinate system $x' - y' - z'$ as $x'_k = x_{mk} - C_{Mx}$, $y'_k = y_{mk} - C_{My}$ and $z'_k = \left[(D/2)^2 - x'^2_k - y'^2_k\right]^{1/2}$. As a high camera frame rate was used, we assume that the orientation of the rotation axis remained nearly unchanged during such a short observation duration of 10^{-2} s. As a result, these five consecutive marker positions would sweep an arc about the rotation axis $\boldsymbol{\psi}$. If we fit a plane E: $z' = A_0 x' + B_0 y' + C_0$ through these markers, the plane surface normal vector $\mathbf{n} = (A_0, B_0, -1)$ should be parallel to the rotation axis $\boldsymbol{\psi}$ that further passes the sphere center. Here, we applied the least-square method to determine the best-fitted $\boldsymbol{\psi}$ so that the radius of gyration r of the swept arc can be further obtained. We then used the line segment between two consecutive marker locations to estimate a mean tangential velocity V and compute the angular speed as $|\boldsymbol{\omega}_p| = V/r$. More details about the rotation dynamics measurement algorithm and its validation can be found in [21].

3 Force measurement and bulk dynamics

3.1 Force measurement for μ_w

A six-axis force sensor (ATI Industrial Automation F/T Sensor Nano17) was mounted into a square window of size 20 mm × 20 mm at the lateral wall. The signal of sensor can be extracted through a data acquisition instruNet DAQ system at a frequency of 5 kHz for 120 s. The voltages were converted into normal and tangential force values, respectively, according to the preliminary calibration relations. The force signals were averaged in time for three

System	M1O1	M1O2	M1O3	M2O1	M2O2	M2O3	M3O1	M3O2	M3O3
M_w (kg)	0.22	0.22	0.22	1.1	1.1	1.1	5.4	5.4	5.4
O (r.p.m.)	5.9	23.4	117.2	5.9	23.4	117.2	5.9	23.4	117.2

Table 1. The flow systems driven with different top loads, M_w, and base rotating rates, O.

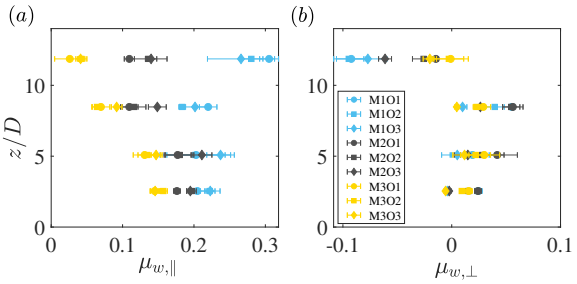

Figure 2. Depth profile for (a) streamwise wall friction coefficient $\mu_{w,\parallel} = \sigma_{r\theta}/\sigma_{rr}$ and (b) transverse wall friction coefficient $\mu_{w,\perp} = \sigma_{rz}/\sigma_{rr}$.

repeated measurements for each flow condition listed in Table. 1.

By changing the force sensor positions at four vertical heights z =15, 30, 50 and 70 mm from the bottom plate (the $z-$coordinate is set at the bottom), we compute the effective wall friction coefficient in the streamwise, $\mu_{w,\parallel} = \sigma_{r\theta}/\sigma_{rr}$, and the transverse, $\mu_{w,\perp} = \sigma_{rz}/\sigma_{rr}$, direction as displayed in Fig. 2. The depth profile of $\mu_{w,\parallel}$ is not uniform but changes primarily with the top load M_w but is less sensitive to the rotating rate O. Under the minimum M_w, $\mu_{w,\parallel}$ remains nearly constant for $z/D < 9$ and then slightly increases close to the top plate. When increasing the M_w, the wall friction coefficient generally decreases with z when approaching the slow shear zone near the top plate and drops to nearly zero for the maximum M_w. For transverse wall friction coefficient, the values are lower than the streamwise coefficient at the three measured points near the base for all conditions. Because the base high-shearing zone is characterized by a dominating horizontal flow, the vertical force is weaker and $\mu_{w,\perp}$ can even become negative near top plate suggesting that the grains exerted downward forces on the wall. In summary, the general decay of μ_w towards the top creep regime has been confirmed in experiments.

3.2 Bulk properties and μ_w degradation models

We used an averaging box of size $(L, W) = (6D, 2D)$ moving by $1D$ along the z-direction to extract the bulk properties across the depth. After spatial averaging of grain dynamics at one depth, the obtained instantaneous bulk properties were averaged in time by the arithmetic mean over 5 seconds. Figure 3(a) shows the depth profile of streamwise velocity scaled by the velocity of the rotating bottom wall, $u_\parallel/OR$, and clear exponential decay profiles are observed in the fast flow regime for all the different flow conditions.

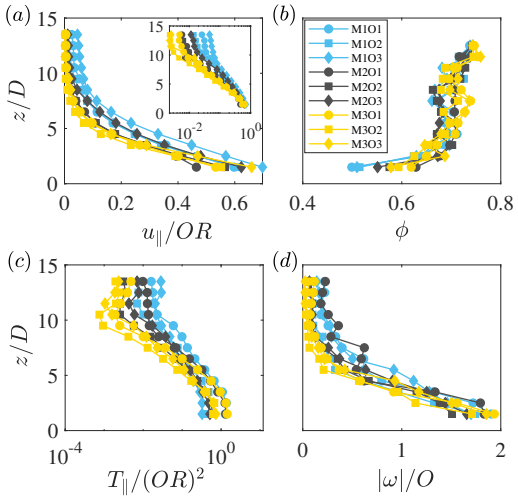

Figure 3. Depth profile for scaled (a) streamwise velocity, (b) volume fraction, (c) streamwise granular temperature and (d) angular velocity.

A greater strength of shear localization with a steeper decay is found when the top load is increased [20] as shown in the inset of Fig. 3(a). In Fig. 3(b), the measured volume fraction remains nearly 0.7 but decreases towards the bottom fast flow regime. Besides, it's worth noting that $\phi(z)$ is slightly increased near the top creep regime (z/D>10).

We then estimate the streamwise granular temperature by

$$T_\parallel = \sum_i \left\{ u_{\parallel,i} - \left[u_\parallel(z_c) + (z_i - z_c) \left.\frac{\partial u_\parallel}{\partial z}\right|_{z_c} \right] \right\}^2 . \quad (3)$$

Here, we account for the velocity gradient at the box center position z_c to eliminate the dependence on the size of the averaging box [22]. The scaled streamwise granular temperature, by O^2R^2, remains nearly constant close to the top wall for each flow condition but increases dramatically when crossing the high-shear zone as shown in Fig. 3(c).

Next, the bulk angular velocity $|\omega|$ was evaluated by the statistic mean—the expected value—within the averaging box. We first collected all the individual grain angular speed $|\omega_p|$ within the averaging box over 5 seconds. We then removed the data falling out of one standard deviation to evaluate the expected value in each box to represent the bulk angular velocity [21]. Scaled by O, Fig. 3(d) shows the depth profile of the scaled bulk angular velocity revealing a roughly exponential-like decay towards the top creep zone.

Finally, we examine the measured data with the two μ_w degradation models in Eq. (1) and (2). The center po-

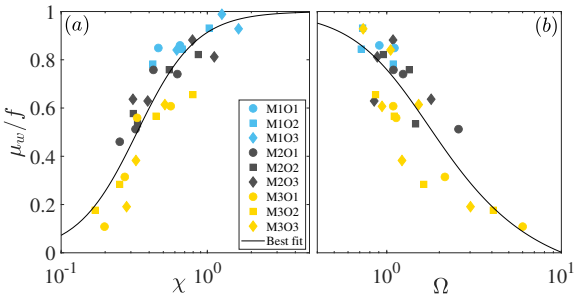

Figure 4. Experimental data of (*a*) $\mu_w/f-\chi$ and (*b*) $\mu_w/f-\Omega$. The solid lines denote the best fitting curve for each corresponding model of Eq. (1) and (2), respectively.

sition of the dynamics averaging box is now placed at the same location with the force sensor. The intrinsic sphere-wall friction coefficient $f = 0.24 \pm 0.01$ is measured by another set of laboratory sliding table tests [23]. As shown in Fig. 4(*a*), monotonically decaying trend for $\mu_w/f - \chi$ is in great agreement with prediction of Eq. (1) with the fitting constants $A = 0.1$ and $B = 2.13$. For the other degradation model in Eq. (2), a decay curve also shows fair agreement to the experimental data with the fitting constants $a = -0.09$ and $b = 0.75$ in Fig. 4(*b*). The negative $a = \omega_\perp/|\boldsymbol{\omega}|$ suggests the streamwise bulk sliding against the sidewall makes grains rotate about the negative z direction which is physically reasonable for the current flow configuration. It surely is desirable to investigate with more information from other flow configurations so that we may bring physical meaning to the fitting coefficients A and B and correlate the dependent variables χ and Ω.

4 Conclusions

In this work, we performed the granular shear cell experiments to confirm the depth-weakening phenomenon of μ_w, compatible with those found in discrete simulations. More interestingly, we compared the measured $\mu_w/f - \chi$ and $\mu_w/f - \Omega$ data to the two existing μ_w degradation models with fitted constants and confirm the effectiveness of both models.

This work provides the first experimental evidence showing the granular temperature and grain rotation are both effective mechanisms to degrade the μ_w. Such finding may suggest the hidden correlation among the two bulk dynamic variables and further link the two boundary condition models in Eq. (1) and (2). The findings shall shed light on future modeling research of the boundary condition of dense granular flows.

5 Acknowledgements

The authors would like to acknowledge the financial support from Ministry of Science and Technology of Taiwan and Campus France, under the Bilateral Orchid Project MOST 107-2911-I-002-536/Campus France 40943RF.

References

[1] P. Mills, D. Loggia, M. Taxier, Europhys. Lett. **45**, 733-738 (1999)
[2] P. Mills, M. Taxier, D. Loggia, Eur. Phys. J. E **1**, 5-8 (2000)
[3] C. Ancey, P. Evesque, Phys. Rev. E **62**, 8349-8360 (2000)
[4] C. Ancey, Phys. Rev. E **65**, 011304 (2001)
[5] C. C. Lin, F. L. Yang, J. Comp. Phys. **420**, 109708 (2020)
[6] K. Hui, P. K. Haff, J. E. Ungar, R. Jackson, J. Fluid Mech. **145**, 223-233 (1984)
[7] P. C. Johnson, R. Jackson, J. Fluid Mech. **176**, 67-93 (1987)
[8] M. W. Richman, Acta Mech. **75**, 227-240 (1988)
[9] J. T. Jenkins, D. Berzi, Granul. Matter **12**, 151-158 (2010)
[10] R. Artoni, A. Santomaso, Granul. Matter **16**, 377-382 (2014)
[11] S. Courrech du Pont, P. Gondret, B. Perrin, M. Rabaud, Europhys. Lett. **61**, 492-498 (2003)
[12] N. Taberlet, P. Richard, A.Valance, W. Losert, J. M. Pasini, J. T. Jenkins, R. Delannay, Phys. Rev. Lett. **91**, 264301 (2003)
[13] P. Jop, Y. Forterre, O. Pouliquen, J. Fluid Mech. **541**, 167-192 (2005)
[14] A. V. Orpe, D. V. Khakhar, J. Fluid Mech. **571**, 1-32 (2007)
[15] P. Richard, A. Valance, J.-F. Métayer, P. Sanchez, J. Crassous, M. Louge, R. Delannay, Phys. Rev. Lett. **101**, 248002 (2008)
[16] N. Brodu, P. Richard, R. Delannay, Phys. Rev. E **87**, 022202 (2013)
[17] R. Artoni, P. Richard, Phys. Rev. Lett. **115**, 158001 (2015)
[18] F. L. Yang, Y. T. Huang, Granul. Matter **18**, 77 (2016)
[19] C. C. Lin, M. Z. Jiang, F. L. Yang, J. Mech. **36**, 707-719 (2020)
[20] R. Artoni, A. Soligo, J.-M. Paul, P. Richard, J. Fluid Mech. **849**, 395-418 (2018)
[21] C. C. Lin, F. L. Yang, Adv. Powder Tech. **29**, 506-517 (2018)
[22] R. Artoni, P. Richard, Phys. Rev. E **91**, 032202 (2015)
[23] S. B. Savage, K. Hutter, Acta Mech. **86**, 201-223 (1991)